PHOTONICS Research

Electron-beam-driven anomalous Doppler effects in Smith–Purcell radiation

Xiaoqiuyan Zhang,[1,2] Tianyu Zhang,[1,2] Zhuocheng Zhang,[1,2] Xingxing Xu,[1,2] Diwei Liu,[1,2] Zhaoyun Duan,[1,2] Yanyu Wei,[1,2] Yubin Gong,[1,2] Liang Jie Wong,[3] and Min Hu[1,2,*]

[1]Terahertz Research Center, School of Electronic Science and Engineering, University of Electronic Science and Technology of China, Chengdu 610054, China
[2]Key Laboratory of Terahertz Technology, Ministry of Education, Chengdu 610054, China
[3]School of Electrical and Electronic Engineering, Nanyang Technological University, Singapore 639798, Singapore
*Corresponding author: hu_m@uestc.edu.cn

Received 13 September 2023; revised 2 November 2023; accepted 2 November 2023; posted 9 November 2023 (Doc. ID 505819); published 21 December 2023

The interaction between electrons and matter is an effective means of light emission, through mechanisms including Cherenkov radiation and Smith–Purcell radiation (SPR). In this study, we show that the superlight inverse Doppler effects can be realized in reverse Smith–Purcell radiation excited by a free electron beam with a homogeneous substrate. In particular, we find that two types of anomalous SPR exist in the homogenous substrate: special SPR and reverse SPR. Our results reveal that the electron velocity can be tuned to simultaneously excite different combinations of normal SPR, special SPR, and reverse SPR. The proposed manifold light radiation mechanism can offer greater versatility in controlling and shaping SPR.

https://doi.org/10.1364/PRJ.505819

1. INTRODUCTION

The scattering of a moving electron's evanescent field off surrounding matter generates a variety of electromagnetic waves [1,2], including Cherenkov radiation (CR) [3–5], Smith–Purcell radiation (SPR) [6–8], and many other forms of radiation [9–12]. These light emission mechanisms have attracted much interest as tunable light sources [13,14], electron detectors [15], and platforms to study the coupling mechanisms between free electrons and materials [16–18]. SPR can be excited in the microwave-to-X-ray range when free electrons pass over the surface of a grating, with the emitted frequency being a function of the angle of radiation, electron beam velocity, and grating period [19]. If the electron velocity exceeds the phase velocity of light in the medium, the electron coupling with this medium generates CR within the Vavilov–Cherenkov (V-C) cone [20,21].

Various inverse effects are sought after due to their fascinating physical properties. Novel light–matter interaction phenomena such as negative refractive index [22,23], reverse Doppler effect [24,25], and reverse CR [26–28] have been theoretically predicted and experimentally observed using artificial electromagnetic materials with left-handed properties, namely metamaterials and photonic crystals. Typically, these anomalous physical phenomena are unattainable in both homogeneous systems. However, a groundbreaking development emerged when Lin *et al.* [24] proposed that the inverse Doppler frequency shift phenomenon could be achieved in homogeneous media, provided that the source speed surpasses twice the speed of light. This extraordinary achievement is called the "superlight inverse Doppler effect" and has sparked a range of captivating studies, including investigations into the positive Doppler phenomenon within negative refractive systems [29].

In this paper, we first prove from Eq. (1) that SPR can be seen as a special Doppler radiation excited by free electrons, bridging the gap between two seemingly unrelated realms. We then propose that anomalous Doppler effects excited by an electron beam lead to anomalous SPR in a structure comprising a grating and a homogeneous substrate with a positive refractive index. Specifically, when the electron beam velocity exceeds the speed of light in the substrate, SPR generated in the V-C cone falls into three categories depending on the velocity of the electron beam and the order of the SPR: normal SPR, special SPR, and reverse SPR. Only normal SPR is excited when the velocity of the electrons is slower than the light velocity in the medium. When the velocity of electrons is greater than the velocity of light in the medium, special SPR and CR will be excited simultaneously. When the electron beam velocity exceeds twice the light velocity in the medium, normal SPR, reverse SPR, and CR will occur simultaneously, as shown in Fig. 1. The field distributions of normal SPR, reverse SPR, and CR in the medium were determined via numerical

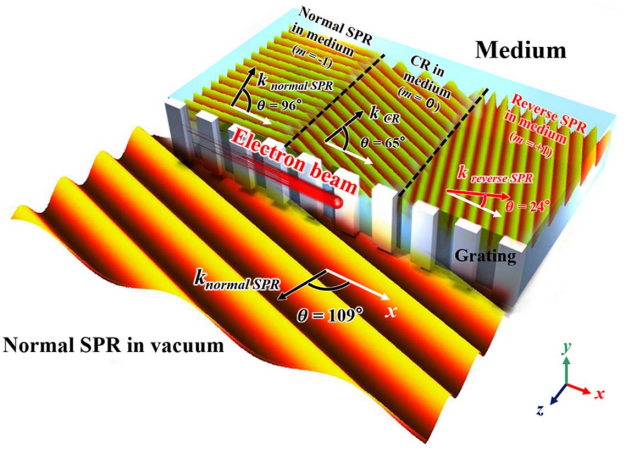

Fig. 1. Schematic of radiative mechanisms arising from electron–matter interactions in a homogeneous material at a single frequency (see Fig. 4 for details of the radiation). The lower half of the image is the normal Smith–Purcell radiation (SPR) in vacuum, in which only negative harmonics electron beams contribute to the evanescent field. In the medium (upper half), normal SPR excited by the −1st harmonic, reverse SPR excited by the 1st harmonic, and Cherenkov (CR) can be present at the same time when the electron velocity is faster than twice the light velocity in the medium. The free electron velocity is 0.6c, with the refractive index n of 4, the grating period of 5 μm, and the radiation frequency of 30 THz.

electromagnetic simulations. In special and reverse SPR, the relationship between the radiation angle and the emitted frequency is opposite to that for normal SPR. In particular, for special and reverse SPR, the emitted frequency within the V-C cone increases with increasing angle from the direction of electron propagation.

2. RESULTS

A. Theory of Normal SPR, Special SPR, and Reverse SPR

We begin with the well-known SPR relation. The frequency f_{SPR} of SPR in a medium at a fixed probe can be calculated as [30]

$$f_{SPR} = \frac{c}{\lambda} = \frac{mu_0}{L}\frac{1}{\beta n\ \cos\ \theta - 1}, \tag{1}$$

where L is the grating period, m is the harmonic number, n is the refractive index of the homogeneous medium, θ is the emission angle from the direction of electron travel, and $\beta = u_0/c$ is the electron velocity u_0 normalized to the speed of light in free space c. The equation indicates that the SPR frequency depends not only on the velocity of the electron and the period of the grating, but also on the angle between the probe and the direction of electron motion. Equation (1) can be contrasted with the Doppler effect equation [9] $\omega(\theta) = \omega_0 \frac{1}{|1-(\frac{u}{c})n(\theta)\cos\theta|}$, where ω_0 is the oscillation frequency in the laboratory reference frame and $\omega(\theta)$ is the frequency of emitted waves. The SPR equation can be seen as a Doppler shift equation for which the emitter frequency is $\omega_0 = |m|u_0/L$. This comparison reveals intriguing parallels between SPR and the Doppler effect and shows that SPR is a potential platform for Doppler effect phenomena to be studied and harnessed.

It should be noted that in vacuum, $n = 1$ and $\beta n\ \cos\ \theta < 1$, so m can only be negative. This means that normal SPR is produced by the coupling of the periodic grating and the evanescent wave of the electron beam in negative space harmonics. $\beta n\ \cos\ \theta = 1$ is the threshold condition for the generation of CR. Thus, when $\beta n\ \cos\ \theta \geq 1$, CR can be excited by an electron beam in the medium. In the homogenous medium, the radiated fields resulting from evanescent fields scattering off the grating manifest as CR and diffraction radiation [31].

To further understand the relationship among the SPR frequency, angle, and velocity of the electron beam, we present the dispersion relation of the periodic structure in Figs. 2(a)–2(c), where the black dashed line is the dispersion of the light line in a vacuum with $k = \omega/c$. Considering a medium with a refractive index n of 4, the light line in the medium is a black solid line with $k = n\omega/c$. From Figs. 2(a)–2(c), it can be seen that the light line moved symmetrically owing to the periodicity of the grating. The colored region bounded by the light cone represents the conditions under which wave propagation is possible. The red dashed lines represent the dispersion relation of the evanescent field from the electron beam, corresponding to different harmonics of the SPR, i.e., $k_{-2} = \omega/u_0 - 4\pi/L$, $k_{-1} = \omega/u_0 - 2\pi/L$, $k_0 = \omega/u_0$, and $k_{+1} = \omega/u_0 + 2\pi/L$, respectively. As shown in Fig. 2(a), the dispersion curve corresponding to the $m = -1$ harmonic and the light line in free space intersect at emission angles of 0° (direction of electron movement) and 180° (direction opposite to electron movement). The emitted frequency at $\theta = 90°$ above the electron can be equivalent to the frequency of the moving electron beam, which is simply the source frequency of Doppler effect $\omega_0 = u_0/L$ (marked by the yellow star in Fig. 2 for $m = -1$).

According to Eq. (1), SPR in a homogeneous medium falls into three categories depending on the value of $\beta n\ \cos\ \theta$. For $\beta n\ \cos\ \theta < 1$ (type 1), the negative harmonics of the grating momentum couple with the electron evanescent field, producing normal SPR; the emission angle ranges from 0° to 180°, with the frequency decreasing at larger angles. For example, normal SPR can be generated in a medium excited by the $m = -1$ harmonic with electron velocity $0.2c$, as shown in Fig. 2(a). The SPR frequency ranges from 6.7 to 60 THz, as the emitted angle ranges from 180° to 0°, when the grating period L is 5 μm. Normal SPR is excited by negative space harmonics because $\beta n < 1$ and m can only be negative, similar to the case of SPR emission into free space. It should be noted that the velocity threshold of CR is $\beta n\ \cos\ \theta = 1$. Therefore, when $\beta n = 1$, CR with a CR angle of 0° is generated from the zeroth space harmonic.

For $1 < \beta n\ \cos\ \theta < 2$ (type 2), normal SPR, special SPR, and CR are simultaneously generated from the $m = -1$, $m = +1$, and $m = 0$ space harmonics, respectively. For example, normal SPR corresponding to the $m = -1$ component of the grating momentum can be generated from an electron of velocity $0.4c$, as shown in Fig. 2(b). According to Eq. (1), when the angle is reduced from 180° to near the angle of the V-C cone $[\theta = \mathrm{acos}(1/\beta n)]$, the frequency of the radiation increases from $\frac{mu_0}{L}\frac{1}{-\beta n-1}$ to infinity. As the angle of radiation is further reduced, after passing through the V-C cone, the

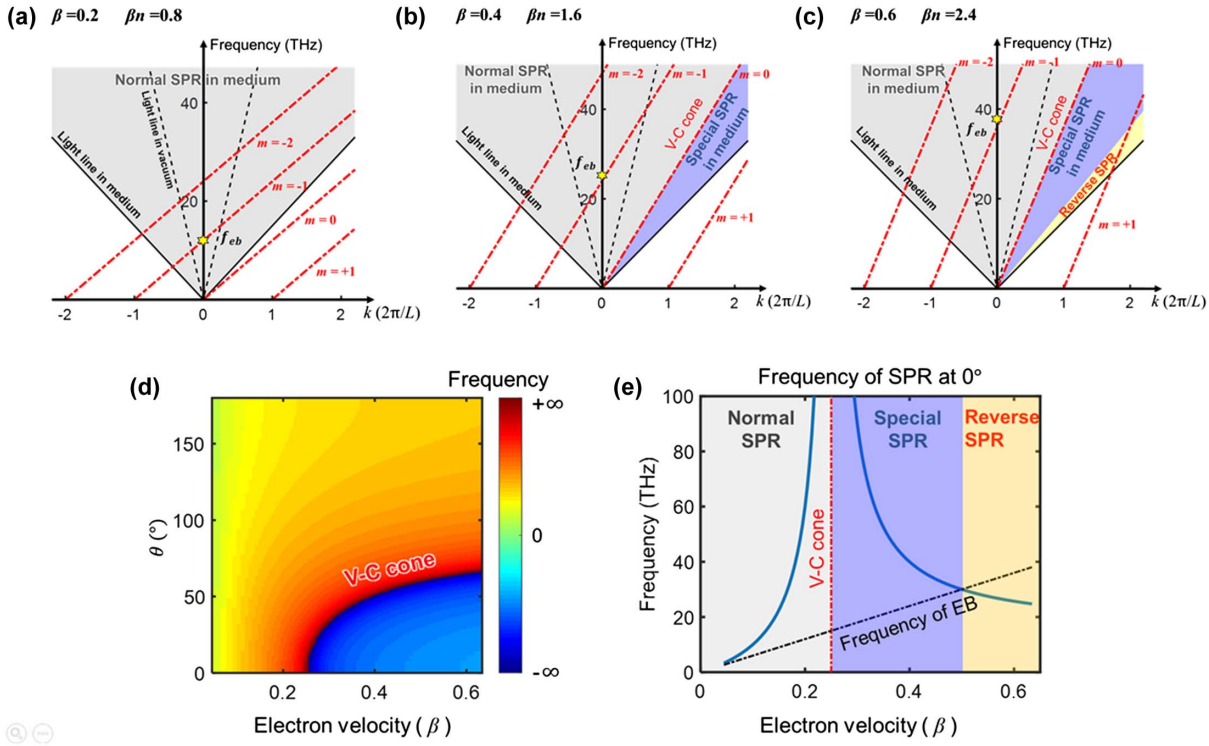

Fig. 2. Dispersion relations for electron velocities of (a) 0.2c, (b) 0.4c, and (c) 0.6c. The black dotted line is the light line in vacuum, and the solid black line is the light line in the medium with a refractive index of 4. The gray area in (a) is normal SPR; the blue area in (b) is special SPR; the yellow area in (c) is reverse SPR. (d) Relationship between the radiation angle and frequency with the refractive index of medium fixed to 4 and electron velocity between 10 eV and 160 keV. (e) Relationship between the frequency of SPR at 0° and electron velocity between 10 eV and 160 keV. The three types of SPR shown in (e) correspond to the dispersion relations shown in (c).

frequency decreases from infinity to $\frac{mu_0}{L}\frac{1}{\beta n-1}$ with an emission angle of 0°. We term this unconventional frequency shift regime special SPR, which is represented by the blue area in Fig. 2(b). It should also be noted that when the angle is greater than $\theta = \text{acos}(1/\beta n)$ and $\beta n \cos\theta - 1 > 0$, the spatial harmonic number m is positive. This reveals an anomalous phenomenon whereby SPR can be excited by positive space harmonics of the grating momentum. From Eq. (1), type 2 radiation satisfies $f_{\text{SPR}} < |m|u_0/L$ with $\cos\theta > 0$. This means that the frequency of the forward-propagating wave of special SPR is always greater than the equivalent frequency of the electron beam. The frequency of SPR at 0° is equal to $|m|u_0/L$ when $\beta n \cos\theta = 2$.

Type 3 SPR satisfies $2 < \beta n \cos\theta$. From Eq. (1), the frequency of the forward-propagating SPR waves can be smaller than the corresponding source frequency $|m|u_0/L$, in accordance with the superlight inverse Doppler effect. This phenomenon, which we term reverse SPR [see Fig. 2(c)], takes place in a conventional right-handed homogeneous material. Both reverse SPR and special SPR are excited by positive space harmonics and exhibit unexpected frequency shifts. In normal SPR and special SPR, the frequency of the forward-propagating wave is always greater than the electronic equivalent frequency of the electron beam; however, in reverse SPR [$\theta > \text{acos}(2/\beta n)$], even the forward-propagating wave can have a frequency lower than that of the source frequency $|m|u_0/L$. For example, reverse SPR in a medium can be excited by $m = 1$ harmonic with a velocity of 0.6c, as shown in Fig. 2(c). The lower frequency of the normal SPR of $|m| = 1$, which is lower than that of the corresponding electronic equivalent frequency, can only produce backward-propagating waves in normal SPR in the medium [see Fig. 2(a)] but can propagate in the forward direction if $2 < \beta n \cos\theta$ [the yellow area in Fig. 2(c)]. The field distribution in Fig. 1 corresponds to that of normal SPR, CR, and reverse SPR in the medium at 30 THz, as shown in Fig. 2(c).

It should be noted that when $2 < \beta n$, the radiation field configuration consists of multiple types of SPR at the same frequency: (1) normal SPR excited by negative space harmonics with $\theta < \text{acos}(1/\beta n)$; (2) special SPR in the V-C cone excited by the 1st space harmonic with $\text{acos}(1/\beta n) < \theta < \text{acos}(2/\beta n)$, or reverse SPR in the V-C cone excited by positive space harmonics with $\text{acos}(2/\beta n) < \theta$; and (3) CR at the V-C cone excited by the zeroth space harmonic with $\text{acos}(1/\beta n) = \theta$, as shown in Fig. 2(c).

In this system, two different phenomena can be explored separately from energy–momentum conservation [32]: a momentum–subtraction SPR excited by negative space harmonics, such as normal SPR, and a momentum–addition SPR excited by positive space harmonics, such as special SPR and reverse SPR, analogous to the superlight inverse Doppler effect [24]. Quantum recoil of SPR should be considered [32] when the initial electron kinetic energy is large enough or the frequency of SPR is high enough with the emission angle θ close to $\cos(1/\beta n)$. In our structure, with electron energy from 0.2c

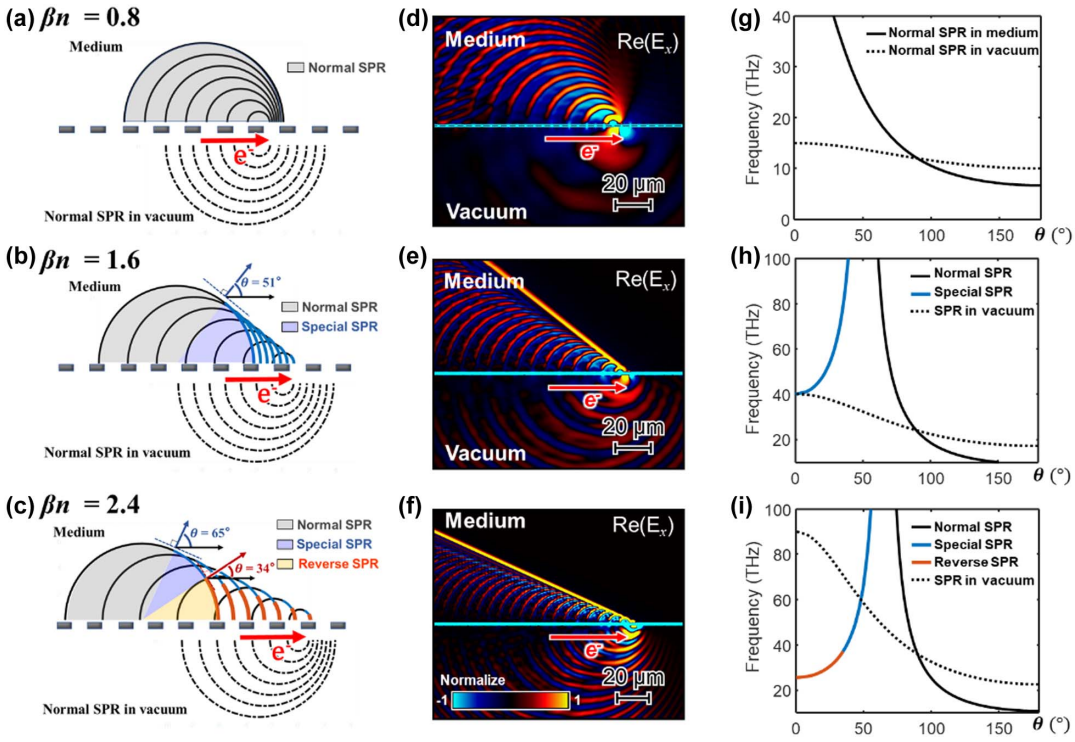

Fig. 3. Schematic of the SPR wavefront with electron beam velocity of (a) 0.2*c*, (b) 0.4*c*, and (c) 0.6*c*. The gray square in the middle is the grating, and the electrons pass through the lower surface of the grating. The upper part of the grating is the medium with $n = 4$, and the lower part is the vacuum. Time-domain contour of the real part of the electric field propagating along the *x* axis E*x* of SPR with electron beam velocity of (d) 0.2*c*, (e) 0.4*c*, and (f) 0.6*c*. Frequency of SPR as a function of the probe angle in medium and vacuum with electron beam velocity of (g) 0.2*c*, (h) 0.4*c*, and (i) 0.6*c*.

to 0.6*c* and the working frequency of 30 THz, quantum recoil can be ignored.

Figure 2(d) shows the relationship between the radiation angle and frequency with the refractive index of the medium fixed to 4 and the electron velocity between 10 eV and 160 keV. Regardless of whether the permittivity index of the medium or the energy of the electrons increases, the positive space harmonics contribute to the electron–matter interactions if the condition $c/n < u_0$ is satisfied. The range of frequency value less than zero in Fig. 2(d) is satisfied for unexpected electron–matter interactions in positive space harmonics. Figure 2(e) shows the frequency emitted at 0° (the blue solid line) as a function of the electron beam velocity. The analysis of the relationship between the emission angle of 0° and the corresponding voltage can enable reverse SPR with the smallest *n*. The method of analyzing other emission angles is the same as that of analyzing 0°. The black dotted line in Fig. 2(e) represents the equivalent frequency of the electron beam, u_0/L, at different voltages. The red dotted line indicates that an electron speed of $0.25c$ is a threshold for a special SPR in the V-C cone. The frequency of the probe in front of the electron beam first increases to infinity and then gradually decreases from infinity as the electron voltage increases. When $0.5c < u_0$, the frequency of SPR observed at 0° is less than the equivalent frequency of electrons, leading to reverse SPR [yellow area in Fig. 2(c)].

B. Simulation of Normal SPR, Special SPR, and Reverse SPR

Next, the particle-in-cell solver of the CST Studio Suite was utilized to study the characteristics of normal SPR, special SPR, and reverse SPR in the V-C cone. We simulated the time-domain contour of the real part of the electric field propagating along the *x* axis E_x of SPR with $n = 4$ and $\beta n = 0.8$, 1.6, and 2.4, respectively [see Figs. 3(d)–3(f)]; to facilitate the analysis, we also drew a schematic of the wavefront of SPR propagating [see Figs. 3(a)–3(c)] and the frequency of SPR in the medium and vacuum [see Figs. 3(g)–3(i)] at the corresponding electron velocity. In this structure, the period *L* of the grating is 5 μm and the gap of the grating is 0.5 μm. For type 1 radiation, normal SPR is generated in the medium, and the frequency shift monotonically decreases with the angle from 0° to 180° [see Figs. 3(a), 3(d), and 3(g)]. For type 2 radiation, normal SPR excited by negative space harmonics and special SPR excited by positive space harmonics were observed in the V-C cone, and the frequency and angle no longer shift continuously [Figs. 3(b), 3(e), and 3(h)]. The simulated V-C cone angle was 51° [see Fig. 3(e)], which is consistent with the theoretical wavefront angle [Fig. 3(b)]. For type 3 radiation, while the frequency and angle no longer change continuously, the low-frequency SPR can produce forward-propagating waves in the 25–38 THz range [see Fig. 3(i)]; this reverse SPR corresponds to the yellow area in Fig. 2(c). However, we noticed

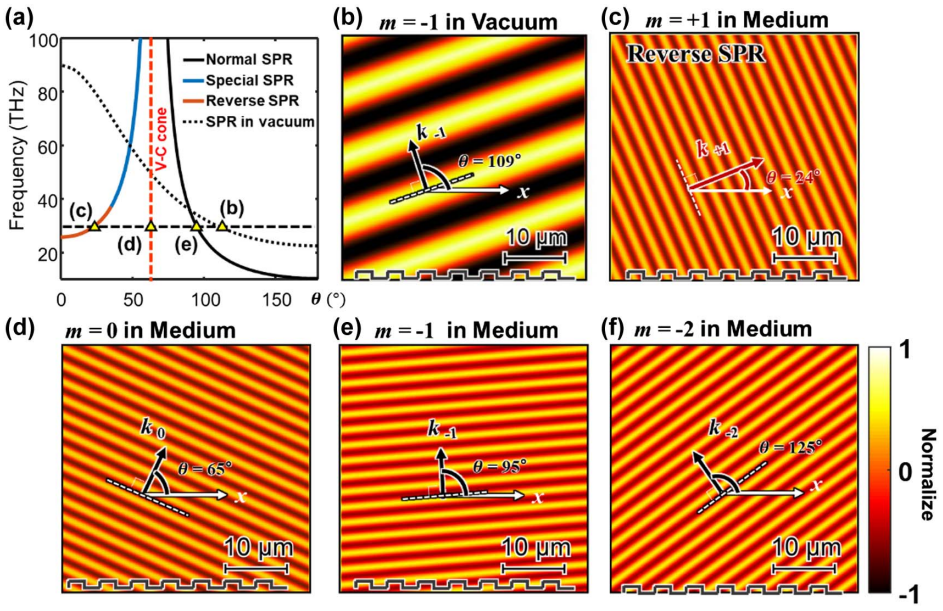

Fig. 4. (a) Frequency of SPR as a function of the angle in a medium and vacuum with electron beam velocity of 0.6*c*. The yellow triangle is the focal point of the black dotted line at $f = 30$ THz and with different types of radiation. The label of each yellow triangle corresponds to the label in (b)–(e). Theoretically calculated field distribution of (b) normal SPR in vacuum, (c) reverse SPR in medium, (d) CR in medium, (e) and (f) normal SPR in medium at 30 THz.

that the normal SPR and CR at the generated V-C cone can be generated at the same time as the reverse SPR. Therefore, it is difficult to directly observe the forward-propagating wave of the reverse SPR using the simulated frequency domain contour results. Thus, we further analyzed the reverse SPR through both calculations and simulations. First, we obtained the radiation field generated by the electron beam of different space harmonics through numerical calculations. Then, the reverse SPR and CR spatially separated from the normal SPR using metasurfaces were directly observed by electromagnetic simulation. The theoretical and simulation results are in excellent agreement.

C. Numerical Calculations of the Radiation Field Generated by Different Space Harmonics

We calculated the field distribution of the 0.6*c* electron velocity excitation grating with a 5 μm period. Owing to the periodicity, the fields in each region can be expanded in space harmonic waves. The wave vector of the space harmonic waves is $k_{xm} = k_x + 2\pi m/L$. The SPR fields excited by different harmonic electron beams can be obtained by matching the boundary conditions [33]. We calculated the field distribution of the SPR in the medium excited by the −1st, 0th, and 1st space harmonics at 30 THz; Fig. 4(a) shows the corresponding distribution at radiation angles of 95°, 65°, and 24°. We also

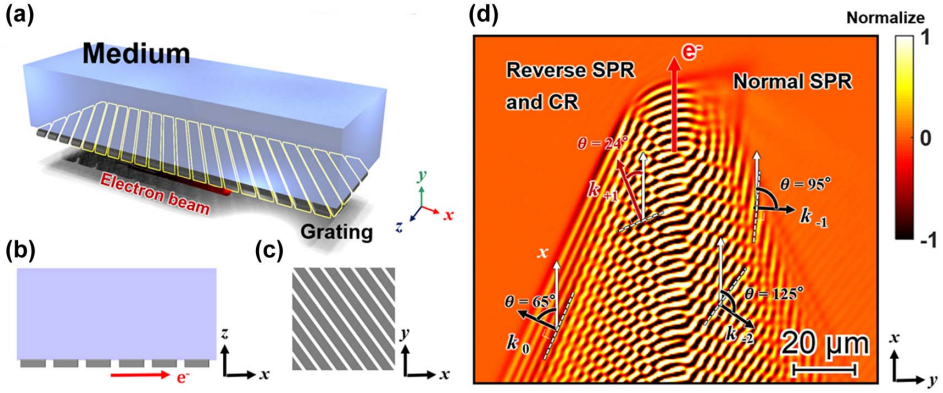

Fig. 5. Schematics of (a) free electron excitation of a metasurface, (b) *XOZ* plane with period *L* and gap *g* of 5 and 0.5 μm, respectively, and (c) *XOY* plane. The metasurface is composed of a 45° angle grating. (d) Direct observation of the simulation of (left) forward-propagation reverse SPR (CR) and (right) backward-propagation normal SPR. The real part of the electric field propagating at 30 THz along the *z* axis is observed at the *XOY* plane 5 μm above the metasurface.

calculated the relationship between the frequency and angle of SPR in vacuum [Fig. 4(a)] and the field distribution at 30 THz [Fig. 4(b)] to compare the SPR in the medium with normal SPR in vacuum. The radiation angle of SPR in vacuum was 109°. From Fig. 4, it can be seen that three different radiations can be excited simultaneously: (1) reverse SPR [Fig. 4(c)] generated by the 1st space harmonic, where the backward-propagating wave of the reverse SPR is opposite to the normal forward-propagating wave of SPR in vacuum [Fig. 4(b)]; (2) normal SPR in the medium [Figs. 4(e) and 4(f)] generated by the −1st and −2nd space harmonics, and (3) the CR at the V-C cone in the medium [Fig. 4(d)] generated by the zeroth space harmonic.

D. Simulation of the Reverse SPR and CR Spatially Separated from the Normal SPR Using Metasurfaces

In combination with a metasurface that enables wavefront modulation [34,35], we directly observe the forward-propagating reverse SPR and the backward-propagating normal SPR in the simulation. A 45° grating was employed as a metasurface to convert the propagation of radiation from forward/backward to right/left [see Fig. 5(a)]; the period L and gap of the grating were 5 and 0.5 μm, respectively [see Figs. 5(b) and 5(c)]. The left side of Fig. 5(d) is the forward-propagating reverse SPR and CR, and the right side shows the normal SPR of the backward-propagation in the medium. It can be seen that the propagating angles of the normal SPR of the −2nd and −1st space harmonics (right) are 125° and 95°, respectively, and that of the reverse SPR (CR) of the 1st and 0th space harmonics (left) is 24° (65°), which are consistent with the theoretical calculation results (Fig. 4).

3. CONCLUSION

In summary, we predict the generation of inverse Doppler effect driven by electron beams in reverse SPR in the V-C cone from electron–matter interactions in a conventional right-handed homogeneous material. Our analytical theory and numerical simulations show that normal SPR, special SPR, and CR can be simultaneously excited by negative, positive, and zeroth space harmonics, respectively, when the electron velocity exceeds the light velocity in the substrate of an SPR grating platform. In special SPR, the frequency shift is blueshifted when the angle increases, which is opposite to the normal SPR redshift. With further acceleration of the electron beam, the normal SPR, special SPR, reverse SPR, and CR can be simultaneously excited if $u_0 > 2v_p$. In reverse SPR, the frequency of the forward-propagating wave is lower than the equivalent frequency of the electron beam, and the conventional backward-propagating wave of normal SPR can be transformed into a forward-propagating wave. The field distributions of normal SPR, reverse SPR, and CR in the medium were determined by numerical calculations and electromagnetic simulations using a metasurface. The reverse SPR in positive harmonic waves is reported for the first time when $u_0 > 2v_p$, although SPR in positive harmonic waves has been studied by Zhang *et al.* [31]. The proposed mechanism of multiple light radiations excited in a conventional right-handed homogeneous material is of great significance for explaining the interaction between electrons and matter. Furthermore, the theory can be extended to negative refractive index systems, which can also produce conventional radiation. In anisotropic materials or other polariton materials, there may be more interesting new physical phenomena excited by electron beams that have not been studied if $u_0 > 2v_p$. Moreover, this phenomenon is expected to assist the development of monochromatic multi-output and high-efficiency tunable radiation sources.

4. MATERIALS AND METHODS

The contour of the real part of the electric field of normal SPR, special SPR, and reverse SPR in the V-C cone was theoretically simulated using the particle-in-cell solver of the CST Studio Suite. A single electron with a length of 6 μm and a charge of 1.6^{-19} C was employed and the electron emission surface was circular, with a radius of 0.2 μm, located above the structure surface. The free electron mode is Gaussian excitation with parameters of 1 μm sigma and 3 μm of cutoff length. It is unnecessary to set a confinement magnetic field because single-electron incidence is considered. Moreover, the electrons can accurately pass through the surface of the grating without hitting it. The boundary conditions in all directions are open.

Funding. Key Laboratory of THz Technology; Fundamental Research Funds for the Central Universities (ZYGX2020ZB007); National Natural Science Foundation of China (61921002, 61988102, 62071108).

Disclosures. The authors declare no conflicts of interest.

Data Availability. Data underlying the results presented in this paper are not publicly available at this time but may be obtained from the authors upon reasonable request.

REFERENCES

1. G. Rosolen, L. J. Wong, and N. Rivera, *et al.*, "Metasurface-based multi-harmonic free-electron light source," Light Sci. Appl. **7**, 64 (2018).
2. C. Roques-Carmes, S. E. Kooi, and Y. Yang, *et al.*, "Free-electron–light interactions in nanophotonics," Appl. Phys. Rev. **10**, 011303 (2023).
3. X. Lin, S. Easo, and Y. Shen, *et al.*, "Controlling Cherenkov angles with resonance transition radiation," Nat. Phys. **14**, 816–821 (2018).
4. Y. Carmel, J. Ivers, and R. E. Kribel, *et al.*, "Intense coherent Cherenkov radiation due to the interaction of a relativistic electron beam with a slow-wave structure," Phys. Rev. Lett. **33**, 1278–1282 (1974).
5. W. D. Kimura, G. H. Kim, and R. D. Romea, *et al.*, "Laser acceleration of relativistic electrons using the inverse Cherenkov effect," Phys. Rev. Lett. **74**, 546–549 (1995).
6. S. J. Smith and E. M. Purcell, "Visible light from localized surface charges moving across a grating," Phys. Rev. **92**, 1069 (1953).
7. S. E. Korbly, A. S. Kesar, and J. R. Sirigiri, *et al.*, "Observation of frequency-locked coherent terahertz Smith-Purcell radiation," Phys. Rev. Lett. **94**, 054803 (2005).
8. S. Huang, R. Duan, and N. Pramanik, *et al.*, "Quantum recoil in free-electron interactions with atomic lattices," Nat. Photonics **17**, 224–230 (2023).
9. V. L. Ginzburg, "Radiation by uniformly moving sources (Vavilov-Cherenkov effect, transition radiation, and other phenomena)," Usp. Fiz. Nauk **166**, 1033 (1996).
10. Z. Gong, J. Chen, and R. Chen, *et al.*, "Interfacial Cherenkov radiation from ultralow-energy electrons," Proc. Natl. Acad. Sci. USA **120**, e2306601120 (2023).

11. J. Chen, R. Chen, and F. Tay, *et al.*, "Low-velocity-favored transition radiation," Phys. Rev. Lett. **131**, 113002 (2023).
12. R. Chen, J. Chen, and Z. Gong, *et al.*, "Free-electron Brewster-transition radiation," Sci. Adv. **9**, eadh8098 (2023).
13. J. Christopher, M. Taleb, and A. Maity, *et al.*, "Electron-driven photon sources for correlative electron-photon spectroscopy with electron microscopes," Nanophotonics **9**, 4381–4406 (2020).
14. G. Kube, H. Backe, and H. Euteneuer, *et al.*, "Observation of optical Smith-Purcell radiation at an electron beam energy of 855 MeV," Phys. Rev. E **65**, 056501 (2002).
15. I. Georgescu, "Light from ripples," Nat. Phys. **8**, 704 (2012).
16. T. Zhang, X. Zhang, and Z. Zhang, *et al.*, "Tunable optical topological transition of Cherenkov radiation," Photonics Res. **10**, 1650–1660 (2022).
17. X. Zhang, M. Hu, and Z. Zhang, *et al.*, "High-efficiency threshold-less Cherenkov radiation generation by a graphene hyperbolic grating in the terahertz band," Carbon **183**, 225–231 (2021).
18. Z. Su, F. Cheng, and L. Li, *et al.*, "Complete control of Smith-Purcell radiation by graphene metasurfaces," ACS Photonics **6**, 1947–1954 (2019).
19. Y. Song, J. Du, and N. Jiang, *et al.*, "Efficient terahertz and infrared Smith–Purcell radiation from metal-slot metasurfaces," Opt. Lett. **43**, 3858–3861 (2018).
20. T. M. Shaffer, E. C. Pratt, and J. Grimm, "Utilizing the power of Cerenkov light with nanotechnology," Nat. Nanotechnol. **12**, 106–117 (2017).
21. J. Tao, L. Wu, and G. Zheng, "Graphene surface-polariton in-plane Cherenkov radiation," Carbon **133**, 249–253 (2018).
22. D. R. Smith and N. Kroll, "Negative refractive index in left-handed materials," Phys. Rev. Lett. **85**, 2933–2936 (2000).
23. D. R. Smith, P. M. Rye, and J. J. Mock, *et al.*, "Enhanced diffraction from a grating on the surface of a negative-index metamaterial," Phys. Rev. Lett. **93**, 137405 (2004).
24. X. Shi, X. Lin, and I. Kaminer, *et al.*, "Superlight inverse Doppler effect," Nat. Phys. **14**, 1001–1005 (2018).
25. J. Chen, Y. Wang, and B. Jia, *et al.*, "Observation of the inverse Doppler effect in negative-index materials at optical frequencies," Nat. Photonics **5**, 239–242 (2011).
26. H. Chen and M. Chen, "Flipping photons backward: reversed Cherenkov radiation," Mater. Today **14**, 34–41 (2011).
27. J. Tao, Q. J. Wang, and J. Zhang, *et al.*, "Reverse surface-polariton Cherenkov radiation," Sci. Rep. **6**, 30704 (2016).
28. X. Guo, C. Wu, and S. Zhang, *et al.*, "Mid-infrared analogue polaritonic reversed Cherenkov radiation in natural anisotropic crystals," Nat. Commun. **14**, 2532 (2023).
29. X. Lin and B. Zhang, "Normal Doppler frequency shift in negative refractive-index systems," Laser Photonics Rev. **13**, 1900081 (2019).
30. A. Massuda, C. Roques-Carmes, and Y. Yang, *et al.*, "Smith–Purcell radiation from low-energy electrons," ACS Photonics **5**, 3513–3518 (2018).
31. P. Zhang, Y. Zhang, and M. Hu, *et al.*, "Diffraction radiation of a subwavelength hole array with dielectric medium loading," J. Phys. D **45**, 145303 (2012).
32. S. Tsesses, G. Bartal, and I. Kaminer, "Light generation via quantum interaction of electrons with periodic nanostructures," Phys. Rev. A **95**, 013832 (2017).
33. T. Zhao, Z. Wu, and M. Hu, *et al.*, "Light radiation from surface plasmon polaritons in a structure of nanometal film on a subwavelength dielectric grating," AIP Adv. **9**, 055219 (2019).
34. X. Zheng, J. Lin, and Z. Wang, *et al.*, "Manipulating light transmission and absorption via an achromatic reflectionless metasurface," PhotoniX **4**, 3 (2023).
35. Y. Hu, X. Liu, and M. Jin, *et al.*, "Dielectric metasurface zone plate for the generation of focusing vortex beams," PhotoniX **2**, 10 (2021).